Symposium: Chemistry at the Nanometer Scale

edited by
K. W. Hipps
Washington State University
Pullman, WA 99163

Electrochemistry at Nanometer-Scaled Electrodes

John J. Watkins, Bo Zhang, and Henry S. White*
Department of Chemistry, University of Utah, Salt Lake City, UT 84112; **white@chem.utah.edu*

An electrochemical reaction is made up of a series of chemical and physical steps occurring at very small length scales *(1)*. The transfer of an electron between the electrode surface and a redox molecule takes place over a distance no greater that 2 nm and occurs in an interfacial region defined by the radius of adsorbed ions and solvent molecules (~1 nm), as well as the distance that surface electric fields extend into the solution (typically 1–100 nm, characterized by the Debye length, κ^{-1}). Prior to the electron-transfer step, the molecule must also be transported from the bulk solution to the electrode surface through the depletion layer, a 0.01–100-μm thick interfacial zone in which the composition of the solution has been altered by the electrochemical reaction. With these length scales in mind, it is natural to consider what new phenomena might occur if the electrode size could be reduced to nanometer dimensions. At such a scale, the electrode is much smaller than the depletion-layer thickness, δ, and comparable to, or even smaller than, the Debye length. It is even reasonable to consider electrodes that approach the size of a redox molecule or the distance that an electron tunnels.

In the late 1970s, analytical chemists first considered the role of electrode size in relation to electrochemical length scales *(2)*. At that time it was recognized that reducing the electrode dimensions (e.g., the radius of an electrode, r) below a critical value of ~10 μm resulted in novel and often remarkable behavior that could immediately be applied in both fundamental and applied chemical analyses. For instance, voltammetry at a microelectrode (an electrode that has one dimension less than ~10 μm) results in a steady-state current–voltage (i–V) response that is much more readily analyzed and employed in chemical analyses than the transient response of a conventional-sized electrode (e.g., 1-mm radius) *(3)*. In addition, microelectrodes can be employed for electrochemical measurements in solutions that do not contain a supporting electrolyte, a possibility that did not previously exist with larger electrodes *(4)*. Although the mathematical description of a microelectrode is fairly complex, both of the above-mentioned advantages can be shown to result from the size of the electrode being smaller than the distance that molecules diffuse in order to reach the electrode surface, that is, $r < \delta$.

In recent years, there has been growing interest in the electrochemical behavior of an electrode when its size is further reduced from the micrometer scale down to the nanometer scale. Disk- and conical-shaped metal electrodes of radius as small as 3 nm have been synthesized and, as shown in a later section, the Faradaic currents at these electrodes are readily measured using standard electrochemical instruments *(5)*. Interest in these ultra-small electrodes is driven partly by a curiosity in understanding how electrochemical behaviors depend on electrode size. For instance, an electrochemical Coulomb staircase has been observed at a 2.8-nm radius electrode *(6)* that is similar to Coulomb blockade in solid-state devices. A nanometer-scaled electrode can also mimic catalytic behavior of Pt particles in fuel cells *(7)*, but has the advantage of being directly electrically wired to current- and potential-measuring instruments. The small size of these electrodes also opens many opportunities in electroanalytical chemistry. For instance, because nanometer-scaled electrodes probe very small regions of a solution, it is possible to detect very small numbers of molecules. The first example of single-molecule electrochemical detection was performed recently using a 15-nm radius Pt electrode *(8)*. Large arrays of nanoelectrodes also offer advantages in the measurement of low concentrations of redox-active molecules *(9)*.

Electrodes of nanometer dimensions are also employed in in-situ electrochemical scanned probe microscopies (e.g., STM), although their electrochemical behavior is not always of primary interest in these applications. One scanned probe microscopy that does make use of the electrochemical properties of such a small electrode is scanning electrochemical microscopy (SECM) *(10–14)*. In SECM, the scanning tip is a metal electrode whose dimensions range from a few nanometers to a few micrometers, depending on the resolution required in a particular experiment. In this application, image interpretation requires a fairly complete understanding of the electrode behavior.

In the remainder of the article, we discuss methods of preparing electrodes of nanometer dimensions and give a few examples of their behavior and applications in relatively simple electrochemical experiments. Before proceeding, it is interesting to note that early applications of metal electrodes of nanometer scale were not in electrochemistry or as a STM tip, but rather in the field of catalysis. For example, in 1985 Elias Greenbaum precipitated colloidal Pt adjacent to the photosystem I reduction site of photosynthesis on a thyalkoid membrane *(15)*. Irradiation of the membrane with light resulted in the splitting of water to hydrogen and oxygen with the nanoscaled Pt electrode, being "wired" to the photosystem, acting as the catalyst. The application of Pt nanoparticles as catalysts in photoelectrochemistry and fuel cells also has a long history *(16, 17)*. What primarily differentiates recent work in this area is the ability to make an electrical connection to a single electrode of nanometer dimensions. Making an electrical connection allows rates and energetics of reactions to be investigated and quantified as a function of the electrode size, as well as allowing individual nanometer-scaled electrodes to be used in a wide range of analytical applications.

Preparation of Electrodes of Nanometer Dimensions

The most common methods found in the literature for preparing metal electrodes of nanoscaled dimensions result in structures that have a band *(18, 19),* cone *(20),* or disk geometry, Figure 1. These electrodes are prepared by methods that vary greatly from laboratory to laboratory. The band electrode (Figure 1A) may be constructed by vapor deposition of a thin layer of either Au or Pt onto a very flat surface, for example, cleaved mica. The topside of the Au layer is coated with an insulating material (epoxy is commonly used) to create a mica–Au–epoxy-layered structure. Simply cutting orthogonally across the mica–Au–epoxy structure then creates a rectangular band-shaped electrode. The width of the electrode, *w*, is determined by the thickness of the Au or Pt layer that was initially deposited onto the mica surface. The lower limit on how small *w* can be is determined by how thin a continuous and conductive metal layer can be deposited on mica. By sputter deposition of Pt or thermal evaporation of Au, electrodes with thicknesses of 2 nm can be prepared that are employable in electrochemical measurements. Thus, it is possible to prepare electrodes that have one dimension, *w*, that is much smaller that the Debye length and that is comparable to the size of the redox molecule as well as the distance of electron tunneling. Band electrodes of width between 2 and 1000 nm have been used to explore near-surface diffusion at the electrode–electrolyte interface *(18).*

Cone- and disk-shaped electrodes of radii that approach a few nanometers can also be prepared using inexpensive materials and instruments. A starting point in preparing either a cone or disk electrode is the electrochemical sharpening of a thin Pt wire. The reason for choosing Pt is that this metal is stable in most electrochemical environments, while many metals, for example, Au, Ag, and Cu, either dissolve rapidly or form a thin oxide layer. Any small quantity of dissolution or change in chemical composition of the surface will wreak havoc with an experimental measurement that employs electrodes of nanometer dimensions.

The methods used to sharpen the Pt wire are identical to those used to sharpen wires for STM tips *(21).* In a typical experiment, a 50-μm diameter Pt wire is suspended in a $CaCl_2$ solution and a moderately large ac voltage (15 V) is applied between the wire and a large counter electrode. Under these extreme conditions, the Pt wire will etch away at the solution–air interface, producing a sharp tip with an angle of ca. 15°. The second step in preparation of a cone or disk electrode is to coat the sharpened wire with an insulating material that is stable in the solution. Nominal cone-shaped nanoelectrodes are prepared by (i) electrochemical deposition of a polymer onto the sharpened Pt wire *(22–24),* (ii) by coating the Pt wire with wax *(6),* and (iii) by pushing the Pt tip through molten glass *(25).* The key to these methods is that the insulating layer (polymer, wax, or glass) is applied in a manner so that it insulates all but the very end of the sharpened wire. For instance, as the polymer film dries in method (i), it contracts to form an electrically insulating, ~100-nm thick layer that is impervious to solvent and ions. Contraction during the drying stage also results in the polymer film retracting away from the sharpened tip, exposing a Pt surface that has roughly a conical shape (Figure 1B). The advantage of this method is that Pt electrodes with very small dimensions (~5 nm) can be prepared relatively easily. A disadvantage is that the polymer film is relatively soluble in organic solvents; thus, applications of these electrodes are limited to measurements in aqueous solutions. The latter limitation is removed by preparation of disk electrodes sealed in glass (Figure 1C). Following a procedure initially developed by Pendley and Abruña *(26),* rather sophisticated capillary pulling instruments have been used to prepare Pt disks with radii as small as 3 nm that are shrouded in glass *(27, 28).* Here we describe a very simple method that can be performed in any chemical laboratory *(29).* A sharpened Pt wire, prepared as above, is sealed in a glass capillary using a H_2/air torch (any standard lab torch will work). Since most glasses melt at temperatures approximately 1000 °C lower than the melting point of Pt (1769 °C), the Pt wire can be sealed in the glass without melting the sharpened tip. Once the Pt is sealed, the end of the glass capillary is then gently polished with decreasing sizes of polishing powders until the very end of the Pt tip is exposed. Whether or not the tip has been exposed is readily determined by placing the electrode in a solution containing a redox-active molecule and recording the voltammetric response. If no Faradaic current is observed, then the Pt has not been exposed and polishing of the electrode is continued. The process is then repeated until a voltammetric current is observed. This trial-and-error procedure is tedious, typically requiring several hours, but the yield of useful electrodes is very good (> 90%). With practice and care, electrodes of radius of 10 nm can be prepared. Because the wire diameter increases as polishing is continued, it is possible to produce any size Pt electrode up to the diameter of the unetched wire. Thus, this method is also an inexpensive and quick means to produce microelectrodes with radii in the 0.1 to 50-μm range.

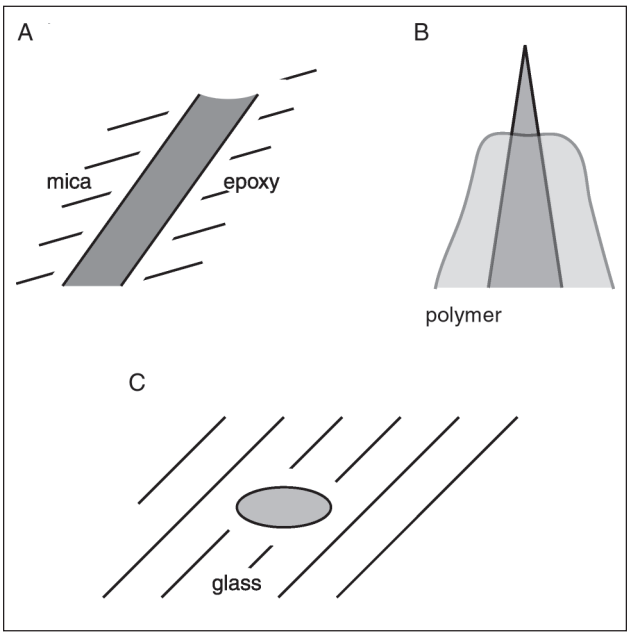

Figure 1. Schematic drawing of (A) band-, (B) cone-, and (C) disk-shaped electrodes.

Electrode Characterization

The preparation of a nanometer-scaled Pt electrode is relatively straightforward. Characterizing the size and shape of such an electrode, however, is a daunting challenge. As will be shown below, if the shape of an electrode is known a priori, then the size can readily determined by measuring the Faradaic current corresponding to the oxidation or reduction of a redox species present in solution at a known concentration. The difficulty is in determining the true shape of the electrode. Electron microscopy is the logical method for examining a small electrode, but has only been employed in a few instances to characterize electrodes with radii less than 100 nm. The difficulty in using electron microscopy is that one is trying to image an individual nanometer-scaled metal electrode that is shrouded by a thick layer of insulating material, Figure 1. Because of this structure, the electrons employed in transmission electron microscopy cannot penetrate through the electrode as needed to acquire an image. In scanning electron microscopy, the entire electrode is first coated by a thin Au film to reduce charging effects associated with imaging an insulating material. However, once the Au film is deposited, it is nearly impossible to locate and then distinguish a flat Pt disk from the surrounding glass.

Several indirect methods of characterizing either the size or shape of nanometer-scaled electrodes have been developed that are based on measuring the electrochemical response of the electrode. For instance, the maximum diffusion-limited current, i_d, obtained at a disk-shaped electrode immersed in an unstirred solution containing a redox species at concentration C^*, is *(3)*

$$i_d = 4nFDC^*r \qquad (1)$$

where n is the number of electrons transferred per molecule, F is Faraday's constant, D is the diffusivity of the redox species, and r is the electrode radius. The diffusion-limited current is easily identified in a voltammogram as the magnitude of the potential-independent current plateau, an example of which will be given below. A value of r is then computed using eq 1 and the experimental value of i_d. Equation 1 is also useful for predicting the current expected at a nanometer-scaled electrode. Assuming a 1-nm radius disk (which is probably the minimum size for making an electrode), a 2 mM concentration, a typical diffusivity of 10^{-5} cm^2/s, and a one-electron redox process, yields i_d = 1 pA. Many commercial electrochemical instruments are readily capable of measuring such a small current. Thus, the application of nanometer-scaled electrodes is rarely limited by the sensitivity of the current-measuring instrument. In more demanding situations, a high-input impedance electrometer has been used to measure currents as small as 10 attoamp (10^{-17} amp) at 3-nm radius electrodes *(6)*.

The use of eq 1 by itself to measure the electrode size is somewhat misleading because the equation is derived based on the assumption that the electrode has a disk geometry and that the electrode is shrouded by a perfectly flat insulating surface. This is nearly impossible to ascertain with certainty without obtaining an electron micrograph. If the electrode has a geometry that is different from a disk, then the numerical factor of 4 in eq 1 is replaced by a different constant. For instance, the diffusion-limited current at hemispherical electrode is *(3)*

$$i_d = 2\pi nFDC^*r \qquad (2)$$

and the factor of 4 is replaced by 2π. Thus, the current at a disk-shaped electrode is a factor of $2/\pi$ smaller than the current at a hemispherical electrode of the same radius. Some researchers are overly concerned with determining the true geometry of the electrode; however, the preceding comparison of a disk and hemispherical-shaped electrodes demonstrates that, in fact, the Faradaic current is not particularly sensitive to the electrode geometry. Thus, in many situations (if not most), the actual geometry is not critical in the final analysis of data. Interpreting the results of an experiment (e.g., measurement of a reaction rate) in which the electrode is erroneously assumed to have a disk shape, when in fact the electrode is hemispherical-shaped, will rarely lead to a numerical error greater than a factor of ~2. This encouraging result relaxes the need for direct observation of the electrode.

Three representative voltammograms recorded at conical-shaped electrodes prepared by the electrophoretic-painting method are shown in Figure 2 *(30)*. The Faradaic current corresponds to the oxidation of ferrocenylmethyltrimethylammonium ion, $FcTMA^+$, present in solution at a concentration of 2 mM. TEM images of the electrodes indicated that the geometry is closer to a hemisphere than a cone. Thus, the radius of the electrodes (70, 17, and 3 nm) were determined using the expression for the diffusion-limited current at a hemisphere, eq 2. As predicted, the Faradaic current at even the 3-nm radius electrode is easily measured, although the noise (0.5 pA) represents about 15% of the diffusion-limited current. In addition, the sigmoidal shape of the voltammetric waves is in exact agreement with theoretical predictions *(3)*. Thus, quantitative i–V data obtained from these electrodes can by employed to investigate the kinetics and energetics of electrode reactions with a relatively high degree of confidence.

There are instances when one needs a more accurate description of the electrode geometry. In such cases, one can measure the area of the electrode by adsorption of a redox-active molecule to form an electroactive film on the electrode surface. Oxidation or reduction of the molecules in the film produces an electrical charge, Q (C), that can then be converted, using Faraday's law ($Q = nFN$, where N is the number of moles of the adsorbed redox molecule) and the surface coverage (Γ, mol/cm^2), to calculate the radius of the electrode (Γ is determined independently by measuring how many molecules adsorb at large electrodes of known radius). If the area of the electrode determined by this method agrees with the value determined from the voltammetric limiting current, then the geometry assumed in analyzing the limiting current is very likely to be correct *(5)*. An alternative method that allows measurement of both the electrode size and shape in the same experiment is to measure the limiting current as the electrode is brought close to a second electrode surface that is macroscopic and flat. This experiment is performed using a scanning electrochemical microscope to position the nanometer-scaled electrode in close proximity to the larger electrode, typical within a distance equal to a few radii of the smaller electrode. The basic idea is that the dif-

fusional flux of molecules between the nanometer-scaled electrode and the larger flat electrode is very sensitive to the geometry of the smaller electrode. Using this procedure, it is possible to determine in a single experiment whether the electrode has the shape of a hemisphere, cone, or disk *(10)*.

The *i–V* Behavior of Nanometer-Scaled Electrodes

The qualitative behavior of a Pt electrode does not vary much as its dimensions are reduced from the micrometer to the nanometer scale. We saw in Figure 2 that a steady-state sigmoidal-shaped voltammetric wave is obtained for the oxidation of $FcTMA^+$ in 0.2 M KCl solutions at Pt electrodes of radius between 3 and 70 nm. The same steady-state wave shape is observed for electrodes with radii up to 10 μm. In addition, the diffusion-limited current, i_d, is proportional to the concentration of $FcTMA^+$ over this entire range of electrode size, in agreement with either eq 1 or 2. However, there are a number of experimental conditions where the nanometer size of the electrode introduces novel behavior. One can generally understand these behaviors by considering the electrode size in relationship to length scales that define the various microscopic steps of an electrochemical reaction *(1)*.

Molecular Transport in the Electrical Double Layer

As the electrode radius approaches nanometer dimensions, a situation arises where the electrical field of the double layer can influence the rate at which molecules are transported to the electrode *(31, 32)*. Consider a Faradaic reaction involving soluble reactants and products, for example, $A^+ + e^- \rightarrow A$. As the reaction proceeds, a thin depletion layer of thickness δ develops in the solution adjacent to the electrode, a consequence of the finite rate at which the reactant can be transported from the bulk to the surface. In order for the reaction to continue, the redox molecule must be transported across this depletion layer to the electrode surface. For a nanometer-scaled electrode, the thickness of the depletion layer, δ, may be comparable to the thickness of the electrical double layer that is established in response to the electrical charge present on the electrode surface, Figure 3. At equilibrium, the Debye length, κ^{-1}, is used to characterize the thickness of the electrical double layer. When κ^{-1} and δ have similar dimensions, the electric field may either enhance or diminish the transport rate of a charged reactant.

The key to understanding why electrode size is important in this problem is in recognizing that the characteristic lengths of the double layer and depletion layer have different dependencies on the electrode size, *r*. In a solution containing a symmetrical *z*:*z* electrolyte, κ^{-1} is proportional to the inverse square root of the ionic concentration, $C^{-1/2}$, but is *independent* of the electrode size, *r (33)*

$$\kappa^{-1} = \left[\frac{kT\varepsilon\varepsilon_0}{2Cz^2e^2}\right]^{1/2} \qquad (3)$$

where ε is the dielectric constant of the solvent, ε_0 is the permittivity of free space, *T* is temperature, k_B is the Boltzman constant, and *e* is the elementary charge. Conversely, the thickness of the depletion layer, δ, is a function of the mode

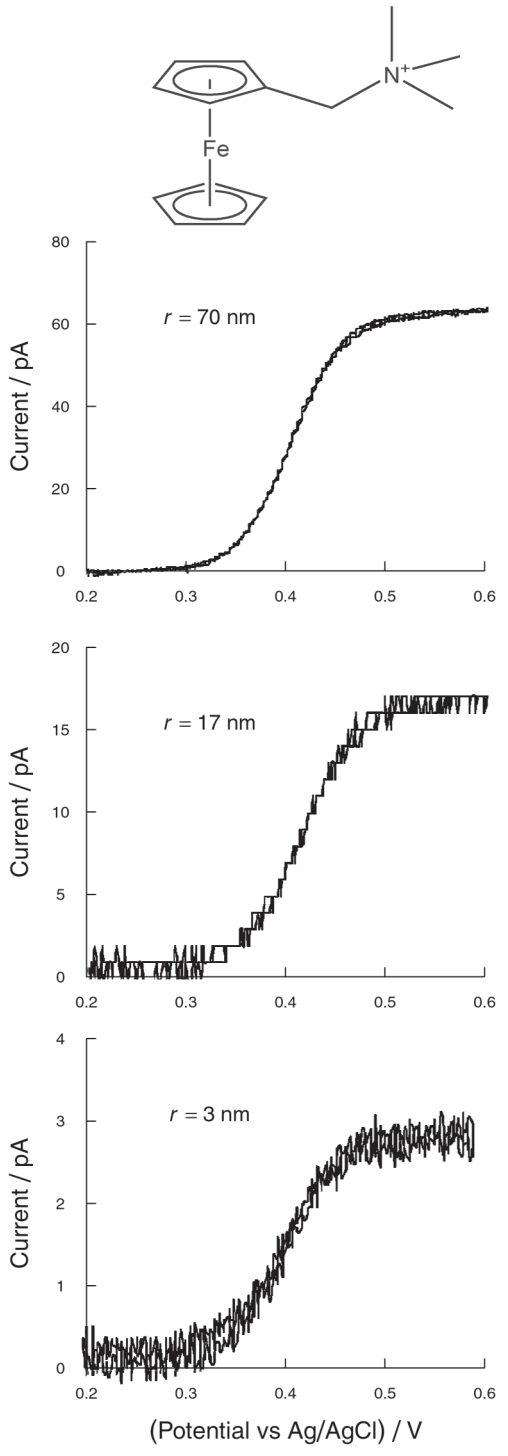

Figure 2. Voltammetric responses of 70-nm, 17-nm, and 3-nm radius hemispherical-shaped Pt electrodes. The current corresponds to the oxidation of 2 mM $FcTMA^+$ in an aqueous solution containing 0.2 M KCl as the supporting electrolyte. The radii of the electrodes were determined from the limiting current using eq 2:

$$i_d = 2\pi nFDC^*r$$

The voltammograms were recorded at a scan rate of 20 mV/s.

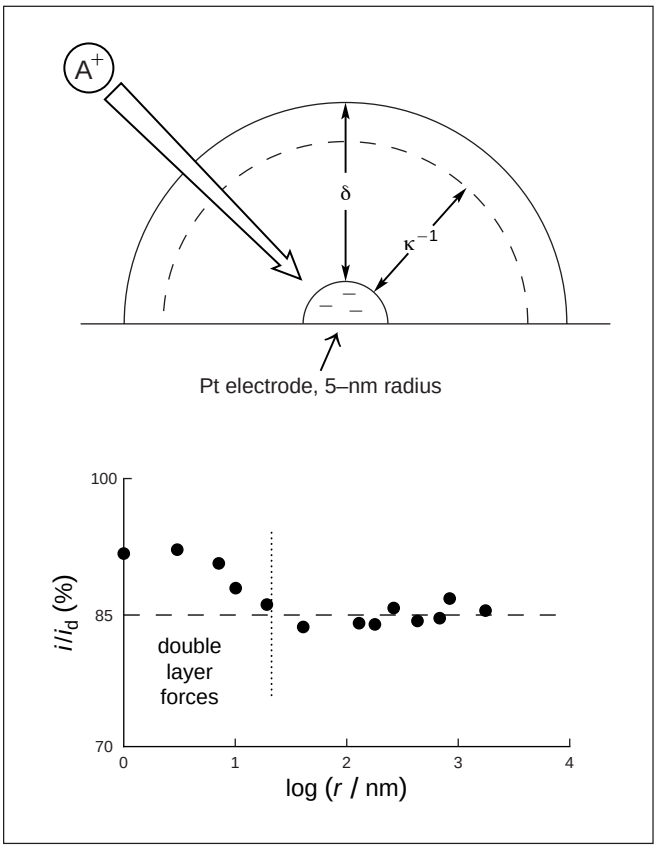

Figure 3. (Top) Schematic depiction of the diffusion layer thickness, δ, and the double-layer thickness, κ^{-1}, for a 5-nm radius electrode immersed in a 0.2 mM 1:1 electrolyte. A charged redox molecule is either electrostatically attracted or repelled by the charge on the surface resulting in enhanced or decreased transport rate, respectively. The schematic shows a positively charged molecule, A^+, attracted to a negatively charged electrode.

(Bottom) Plot of the normalized diffusion-limited current, i/i_d, as a function of electrode radius for the oxidation of $FcTMA^+$.

of transport (diffusion, migration, convection), as well as the electrode geometry *and size*, *r*. For a hemispherical electrode δ!m)n be approximated as

$$\delta = 5r \qquad (4)$$

The factor of 5 in eq 4 defines δ as the distance from the center of the electrode to a distance in solution where the concentration of the reactant is equal to 80% of its bulk value [strictly true for diffusion-controlled molecular transport *(33)* and a good approximation even when migration is operative].

For a macroscopic electrode in a solution containing an excess concentration of electrolyte, κ^{-1} is a negligible fraction of δ and the electric field within the double layer has an insignificant effect on the transport of redox molecules to the electrode. However, κ^{-1} becomes comparable to δ when the electrode is reduced to nanometer dimensions. When $\kappa^{-1} \sim \delta$, the electric field at the electrode is expected to accelerate or retard the flux of ions to the surface. For instance, Figure 3 depicts the steady-state reduction of A^+ at a negatively charged electrode of 5-nm radius in a solution containing a 1:1 electrolyte at a concentration of 2×10^{-4} M. This concentration corresponds to $\kappa^{-1} \sim 20$ nm; the electric field will decay to ~95% of its value at the surface at $3\kappa^{-1}$ (= 60 nm). The thickness of the depletion layer is ~5*r* or only 25 nm (eq 4). Thus, an attractive electrostatic force between the negatively charged electrode and the positively charged reactant is anticipated to accelerate the transport of A^+ to the electrode surface, thus increasing the Faradaic current. Conversely, if the reactant is negatively charged, A^-, the flux to a negatively charged electrode is anticipated to be impeded, resulting in a decreased current.

The above ideas were tested by measuring the limiting current for the oxidation of $FcTMA^+$ at Pt electrodes of radius between 2 and 2000 nm. To observe the influence of the double-layer electric field on transport, the voltammetric current for the oxidation of 2 mM $FcTMA^+$ was measured in the presence and absence of a supporting electrolyte, 0.1 M KCl. (Note that when a supporting electrolyte is present, the current is diffusion-controlled and equal to i_d as defined by eq 2. A well-defined sigmoidal voltammogram is obtained in both the presence and absence of a supporting electrolyte.) In the absence of the supporting electrolyte, κ^{-1} is determined by the concentration of the charged redox species, $FcTMA^+$, and its counterion, PF_6^-, which yields an approximate double-layer thickness of $3\kappa^{-1} \sim$ 20 nm. In the presence of 0.1 M KCl, the double layer is much thinner, $3\kappa^{-1} \sim 3$ nm.

The lower portion of Figure 3 shows a plot of ratio of the transport-limited current in the absence and presence of the supporting electrolyte, i/i_d, as a function of electrode size. The dashed line is the predicted theoretical value of this ratio when double-layer fields are absent. Values of i/i_d agree well with the theoretical value for electrodes of radius greater than ca. 10 nm. Below this value, the current in the absence of the supporting electrolyte increases, suggesting an attractive force between the reactant, $FcTMA^+$, and the electrode surface. The result is consistent with a *negatively charged electrode*. To test this conclusion, the experiment was repeated using a neutral

ferrocene,1,1′-ferrocenedimethanol, $Fc(CH_2OH)_2$, and a negatively charged ferrocene, ferrocene monocarboxylate, $FcCOO^-$. Values of i/i_d for oxidation of $FcCOO^-$ *decrease* as the electrode size is reduced below 10 nm, while no dependence of i/i_d on r is observed for the neutral species, $Fc(CH_2OH)_2$ *(34)*. The diminishment and enhancement of the Faradaic currents for the anion and cation, respectively, confirm that a negative charge exists on the Pt surface at potentials where the ferrocenes are oxidized (ca. 0.5 V vs Ag/AgCl).

The Influence of Interfacial Potential Distribution on Electron-Transfer Rates

In the preceding example, the rate at which the different charged ferrocenes were oxidized was determined solely by how fast they could be transported to the electrode surface. In this limiting case, the electron-transfer step can be considered to be infinitely fast and has no effect on the shape of the voltammetric wave. In many systems, however, electron transfer is the rate-limiting step. When this occurs, a larger driving force (i.e., electrode potential) is required in order to overcome the kinetic limitation.

The sequential nature of the mass and electron-transfer steps for a generic reaction, $A^+ + e^- \rightarrow B$, can be represented as follows:

$$A^+_{bulk} \xrightarrow[(D/r)]{\text{mass transfer}} A^+_{surface} \xrightarrow[(k)]{\text{electron transfer}}$$

$$B_{surface} \xrightarrow[(D/r)]{\text{mass transfer}} B_{bulk}$$

The electron-transfer rate constant, k (cm/s), is a function the molecular species, the electrode material, the solvent, and supporting electrolyte and varies over many orders of magnitude *(33)*. On the other hand, the rate of mass transfer is characterized by a coefficient that is a function of the electrode geometry and size. For a spherical electrode, the mass-transfer coefficient is given by D/r (cm/s) *(33)*, which indicates that the rate of molecular transport increases in inverse proportion to the electrode radius, $1/r$. Thus, as r is decreased to smaller and smaller values, the reaction will eventually become limited by the rate of the electron-transfer step. When the electron-transfer step becomes rate limiting, the i–V waveshape can be analyzed to extract k. This strategy has been used for many years to measure the rate of electron-transfer reactions *(35)*.

The condition required for the electron-transfer step to be rate limiting is that $k << D/r$, which is generally expressed in the literature as:

$$\frac{D}{kr} \geq 0.1 \qquad (5)$$

Thus, in principle, assuming a typical value of D (~10^{-5} cm^2/s), it is possible to measure values of k as large as ~300 cm/s using the smallest Pt electrodes currently available (~3 nm).

To illustrate the use of this strategy, consider the simple one-electron outer-sphere oxidation of $Ir(Cl)_6^{3-}$ at Pt. In the presence of a supporting electrolyte, for example, 0.1 M KCl, the reaction is very fast ($k \sim 5$ cm/s) and is difficult to measure by conventional electrochemical methods. The value of k is also a function of the concentration of the supporting electrolyte, a consequence of the fact that the driving force for electron transfer depends on magnitude of the electrostatic potential drop between the electrode and the plane of electron transfer (PET), the latter corresponding to the distance between the redox molecule and the electrode at the moment of electron transfer (i.e., the tunneling distance). As shown in Figure 4, the driving force for electron transfer corresponds to $(\phi^S - \phi^{PET})$, which represents the difference between the electrostatic potential at the electrode, ϕ^S, and in the solution at the PET, ϕ^{PET}. Similar to the Debye length, κ^{-1}, the value of $(\phi^S - \phi^{PET})$ is a function of the supporting electrolyte concentration, decreasing as the ionic strength is lowered as shown in Figure 4.

Although this is not completely understood, values of k for some redox reactions are very sensitive to $(\phi^S - \phi^{PET})$ while others are not. The oxidation of $Ir(Cl)_6^{3-}$ is an example of a redox reaction whose kinetic rate is particularly sensitive to $(\phi^S - \phi^{PET})$, as demonstrated in the lower part of Figure 4.

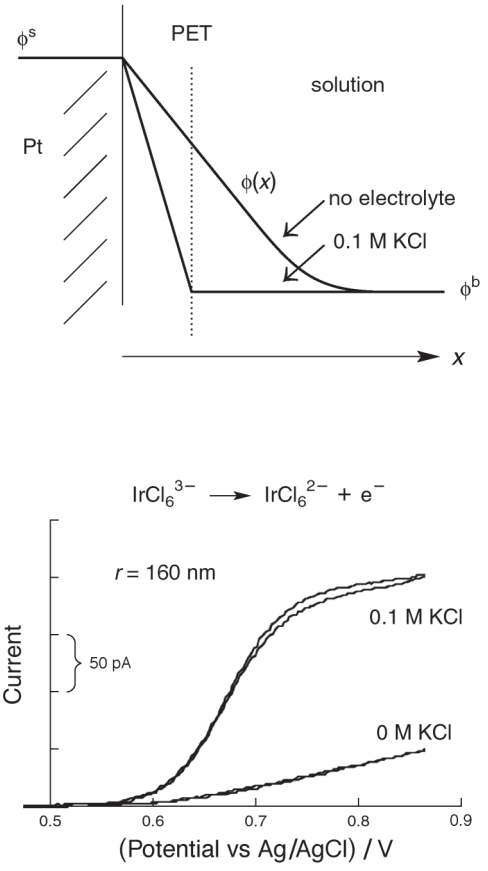

Figure 4. (Top) Schematic diagram of the potential distribution as a function of distance, x, at the electrode–electrolyte interface in the presence and absence of a supporting electrolyte (e.g., 0.1 M KCl). The driving force for electron transfer, $\phi^S - \phi^{PET}$, is a function of the electrostatic potential, $\phi(r)$, at the plane of electron transfer (PET). Lower ionic concentrations results in smaller values of $\phi^S - \phi^{PET}$. (Bottom) Steady-state voltammograms corresponding to the oxidation of $IrCl_6^{3-}$ at a 160-nm radius Au electrode in the presence and absence of a supporting electrolyte. The drawn-out i–V response in the absence of electrolyte is due to a decreased driving force for electron transfer.

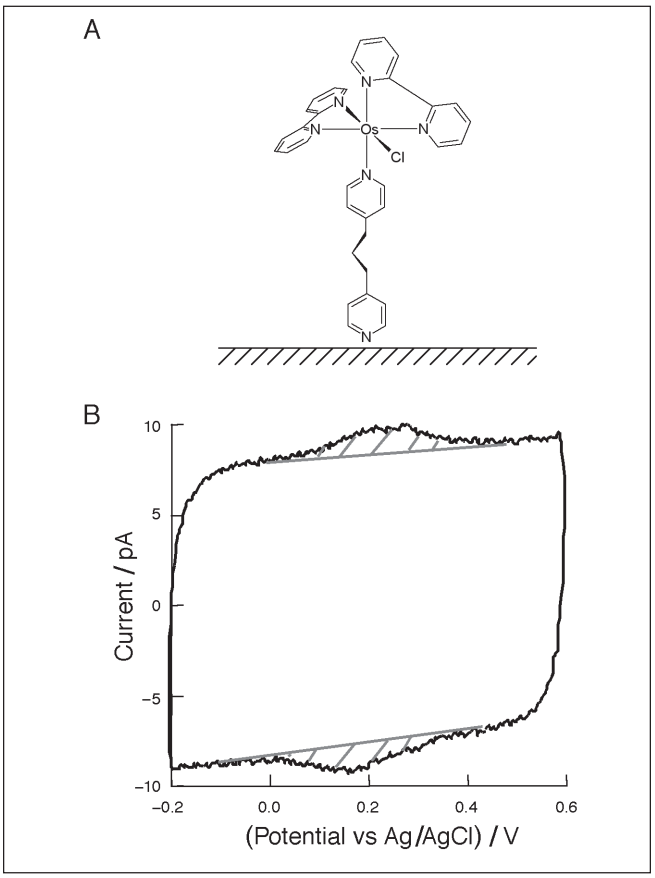

Figure 5. Illustration of the use of nanometer-scaled electrodes in detecting a very small number of molecules.

(A) Schematic of $Os(bpy)_2(dipy)Cl^+$ adsorbing at Pt.

(B) Cyclic voltammogram at 1000 V/s (200 waveforms averaged) corresponding to the oxidation and re-reduction of $Os(bpy)_2(dipy)Cl^+$ adsorbed at a Pt electrode (r = 170 nm) immersed in a 0.2 M $NaClO_4$ solution. The small waves shaded in gray are due to oxidation and re-reduction of $Os(bpy)_2(dipy)Cl^+$. The large background current is due to stray capacitance.

In this set of experiments, a 160-nm radius Au electrode was used to record the *i–V* response corresponding to the oxidation of $Ir(Cl)_6^{3-}$ in the presence and absence of 0.1 M KCl. In the presence of the supporting electrolyte, the *i–V* responses has the classic sigmoid shape that is characteristic of a reaction limited solely by molecular transport, i.e., $k >> D/r$. Indeed, the electron-transfer rate is immeasurable fast for these solution conditions at a 160-nm radius electrode. On the other hand, when the supporting electrolyte is not present, the *i–V* response becomes drawn out, suggestive of slow electron transfer, $k << D/r$. Since D is not very sensitive to the electrolyte concentration, and since the same electrode is used in recording the two responses in Figure 4 (i.e., D/r is constant), it follows that the change in the voltammetric response is due to a decrease in k when the electrolyte is removed. In more systematic studies, the *i-V* response can be used to determine k as a function of electrolyte concentration, as well as to estimate the corresponding values of $(\phi^S - \phi^{PET})$ *(36)*. This type of data would be impossible to obtain using larger electrodes for several reasons. First, although the reaction appears sluggish in the absence of an electrolyte at the 160-nm radius electrode, it is still sufficiently fast that mass transfer would be rate limiting at any electrode of radius greater than ca. 10 μm. Second, it is impossible to perform quantitative kinetic measurements in the absence of an electrolyte using macroscopic electrodes owing to the large Ohmic potential drop in solution. Thus, the kinetics of the $IrCl_6^{3-}$ system are only assessable using electrodes of nanoscaled dimensions.

Detection of Small Numbers of Molecules

Electrochemical detection of very small numbers of molecules is difficult because of the problems associated with counting electrical charge (as opposed to counting photons) and because of the large background currents associated with impurities and the stray capacitances. One way to reduce the background current is to simply reduce the size of the electrode. Using smaller electrodes also results in a decrease in the number of molecules being probed (this strategy is analogous to diluting a sample containing a dye molecule in order to observed fluorescence from a single molecule).

To illustrate the use of nanometer-scaled electrodes in detecting a very small number of molecules, consider an experiment in which a redox-active molecule, $Os(bpy)_2(dipy)Cl^+$, is adsorbed at a nanoscaled Pt electrode. $Os(bpy)_2(dipy)Cl^+$ adsorbs at Pt as depicted in Figure 5, forming a close-packed monolayer with a surface coverage of ~0.7 molecule/nm^2, independent of electrode area. Once adsorbed, this complex undergoes a reversible one-electron oxidization, generating a Faradaic current that can be integrated and used, in conjunction with Faraday's law, to compute the number of molecules sitting on the surface.

The size of the electrode determines the number of molecules that will be detected in this experiment. Thus, one could optimistically imagine the detection of one molecule of $Os(bpy)_2(dipy)Cl^+$ adsorbed at a 1-nm radius electrode. However, as the electrode size is decreased, the Faradaic current, which is proportional to the number of molecules, will eventually decrease below the background current or instru-

ment noise. One way to beat the instrument noise is to scan the electrode potential at high scan rates, as the Faradaic current for oxidation–reduction of an adsorbed redox molecule increases in proportion to scan rate *(37),* while the instrument noise is much less dependent of the scan rate. An example of the fast-scan voltammetric response (n = 1000 V/s, average of 200 scans) of a 170-nm radius Pt electrode at which a monolayer of $Os(bpy)_2(dipy)Cl^+$ has been adsorbed is shown in Figure 5. Voltammetric waves associated with oxidation and reduction of $Os(bpy)_2(dipy)Cl^+$ are clearly discernible (shaded in gray), although they are already minuscule in comparison to the large background charging current associated with stray capacitances. Unfortunately, the background charging current also increases linearly with scan rate and cannot be reduced without eliminating the source of the stray capacitance. Integration of the shaded region of the voltammetric wave yields an electrical charge of $Q = 3.8 \times 10^{-14}$ C, which corresponds to ~2×10^5 molecules. Similar measurements using a 70-nm radius electrode yield an electrical charge of 1.1×10^{-15} C, corresponding roughly to 7,000 molecules or 1.1×10^{-20} mole (~10 zeptomole) *(5).*

Spectroscopists are quick to point out that 10 zeptomole represents a large number of molecules in comparison to a single molecule that can routinely be detected by a number of optical methods. However, a zeptomole represents a very small number of molecules in an electrochemical measurement. Furthermore, there is lots of room for improvement in instrument design, as well as many unexplored strategies for achieving single-molecule detection in electrochemistry. As noted previously, the ultimate limit of electrochemical detection has been demonstrated by trapping a single redox molecule between a 15-nm radius SECM Pt tip and a large Pt electrode *(8).* Rapid diffusional cycling of the molecule back and forth between the Pt tip and the large Pt electrode, where it is oxidized and reduced, respectively, at a rate of 10^6 events/s, results in a very small but measurable current. This is a difficult experiment and, unlike conventional voltammetric measurements described above, is unlikely to be used in routine analysis. However, it clearly demonstrates how novel opportunities emerge in chemical analysis by simple reducing the size of the electrode to nanometer dimensions.

Conclusions

Advances in the fabrication of nanometer-scaled electrodes during the past decade have created a number of opportunities in both physical chemistry and analytical measurements. Electrochemical studies using these electrodes are already leading to better insights into electrochemical kinetics, interfacial structure, and chemical analysis. Analogous to many areas of nanoscience, much work on improving fabrication and characterization procedures is required before widespread applications of such small electrodes are possible. Nevertheless, the many unique advantages of making electrochemical measurements on the nanometer scale will make this a very fruitful area of future research.

Acknowledgment

The authors thank the Office of Naval Research for financial support of research on nanometer-scaled electrodes.

Literature Cited

1. Faulkner, L. R. *J. Chem. Educ.* **1983,** *60,* 262.
2. Wightman, R. M. *Anal. Chem.* **1981,** *53,* 1125A.
3. Zoski, C. G. In *Modern Techniques in Electroanalysis;* Vanysek, P., Ed.; Wiley: New York, 1996.
4. Amatore, C.; Fosset, B.; Bartlett, J.; Deakin, M. R.; Wightman, R. M. *J. Electroanal. Chem.* **1988,** *256,* 255.
5. Watkins J. J.; Chen. J.; White, H. S.; Abruña, H. D.; Amatore, C. *Anal. Chem.* **2003,** *75,* 3962.
6. Fan, F. R. F.; Bard, A. J. *Science* **1997,** *277,* 5333.
7. Chen, S.; Kucernak, A. *J. Phys. Chem. B* **2004,** *108,* 3262.
8. Fan, F. R. F.; Bard, A. J. *Science* **1995,** *267,* 871.
9. Menon, V. P.; Menon, Martin, C. R. *Anal. Chem.* **1995,** *6,* 1920.
10. Bard, A. J.; Mirkin, M. V. *Scanning Electrochemical Microscopy;* Marcel Dekker: New York, 2001.
11. Mirkin, M. V. *Anal. Chem.* **1996,** *68,* 177A.
12. Gardener, C. E.; Macpherson, J. V. *Anal. Chem.* **2002,** *74,* 576A.
13. Macpherson, J. V.; Unwin, P. R. *Anal. Chem.* **2000,** *72,* 276.
14. Abbou, J.; Demaille, C.; Druet, M.; Moiroux, J. *Anal. Chem.* **2002,** *74,* 6355.
15. Greenbaum, E. *Science* **1985,** *230,* 1373.
16. Watanabe, W.; Motto, S. *Electroanal. Chem. Interface Electrochem.* **1975,** *60,* 275.
17. Aspnes, D. E.; Heller, A. *J. Phys. Chem.* **1983,** *87,* 4919.
18. Morris, R. B.; Franta, D. J.; White, H. S. *J. Phys. Chem.* **1987,** *91,* 3559.
19. Nagale, M. P.; Fritsch, I. *Anal. Chem.* **1998,** *70,* 2908.
20. Zoski, C. G.; Mirkin, M. V. *Anal. Chem.* **2002,** *74,* 1986.
21. Melmed, A. J. *J. Vac. Sci. Technol. B* **1991,** *9,* 601.
22. Slevin, C. J.; Gray, N. J.; MacPherson, J. V.; Webb, M. A.; Unwin, P. R. *Electrochem. Commun.* **1999,** *1,* 282.
23. Chen, S.; Kucernak, A. *J. Phys. Chem. B* **2002,** *106,* 9396.
24. Sun, P.; Zhang, Z.; Guo, J.; Shao, Y. *Anal. Chem.* **2001,** *73,* 5346.
25. Penner, R. M.; Heben, M. J.; Lewis, N. S. *Anal. Chem.* **1989,** *61,* 1630.
26. Pendley, B. D.; Abruña, H. D. *Anal. Chem.* **1990,** *62,* 782.
27. Shao, Y.; Mirkin, M. V.; Fish, G.; Kokotov, S.; Palanker, D.; Lewis, A. *Anal. Chem.* **1997,** *69,* 1627.
28. Katemann, B. B.; Schuhmann, W. *Electroanalysis* **2002,** *14,* 22.
29. Zhang, B.; Zhang, Y.; White, H. S. *Anal. Chem.* **2004,** *76,* 6229.
30. Conyers, J. L.; White, H. S. *Anal. Chem.* **2000,** *72,* 4441.
31. Norton, J. D.; White, H. S.; Feldberg, S. W. *J. Phys. Chem.* **1990,** *94,* 6772.
32. Smith, C. P.; White, H. S. *Anal. Chem.* **1993,** *65,* 3343.
33. Bard, A. J.; Faulkner, L. R. *Electrochemical Methods;* 2nd ed.; John Wiley & Sons, Inc.: New York, 2001.
34. Watkins, J. J.; Cope, B. D.; Conyers, J., Jr.; White, H. S. In *Interfaces, Phenomena, and Nanostructures in Lithium Batteries;* Klingler, Robert, Ed.; Electrochemical Society: Princeton, NJ, 2001; Vol. 2001–36, p 163.
35. Penner, R. M.; Heben, M. J.; Longin, T. L.; Lewis, N. S. *Science* **1990,** *250,* 1118–1121.
36. Watkins, J. J.; White, H. S. *Langmuir* **2004,** *20,* 5474.
37. Hudson, J.; Abruña, H. D. *J. Phys. Chem.* **1996,** *100,* 1036–1042.